Spectroscopy of Hydrothermal Reactions. 7. Kinetics of Aqueous $[NH_3OH]NO_3$ at 463−523 K and 27.5 MPa by Infrared Spectroscopy

J. W. Schoppelrei and T. B. Brill*

Department of Chemistry, University of Delaware, Newark, Delaware 19716

Received: July 23, 1997; In Final Form: September 17, 1997[⊗]

The first kinetic measurements for aqueous $[NH_3OH]NO_3$ that are based on species concentrations at hydrothermal conditions are discussed. The decomposition rate of 0.1 and 0.2 *m* $[NH_3OH]NO_3$ was determined in real time by flow-cell IR spectroscopy at 463−523 K and 27.5 MPa. The loss of NH_3OH^+ (2730 cm^{-1} bending combination) and formation of N_2O (ν_3 at 2230 cm^{-1}) occur at the same rate under these conditions and were fit to a first-order rate expression. Using all of the data, $E_a = 103 \pm 21$ kJ/mol and $\ln(A/s) = 21 \pm 5$. The decomposition rate resembles that of solid $[NH_3OH]NO_3$ in a similar temperature range, but the kinetics for dilute solutions and the solid state are too slow to apply to the combustion rate of a more concentrated solution of $[NH_3OH]NO_3$.

Introduction

A highly concentrated aqueous solution of hydroxylammonium nitrate, $[NH_3OH]NO_3$, mixed with alkylammonium nitrate salts burns very rapidly, which makes it useful as a liquid propellant.[1−3] In fact, even approximately 40 wt % of $[NH_3OH]NO_3$ in water (5 M) will burn steadily provided that the pressure is greater than 5 MPa.[4] A phenomenological model describing this deflagration process has been developed.[5] The controlling event is believed to be the rate of decomposition of $[NH_3OH]NO_3$ in the condensed phase. Therefore, the kinetics and pathway of decomposition in water at high temperature and pressure are of interest. The main problem is, however, that the reaction is highly exothermic, which makes it difficult to control during the investigation. Thus, although $[NH_3OH]NO_3$ dissolves up to 95 wt % in water,[6] the use of a dilute solution has been necessary to measure the reaction rate.

Recent development of spectroscopy/flow cells suitable for real-time IR and Raman studies at hydrothermal conditions (T = 450−620 K, P = 27.5 MPa) make direct spectrokinetic measurements now feasible.[7−9] Described herein is a real-time investigation of the decomposition rate of 0.1 and 0.2 *m* $[NH_3OH]NO_3$ (*m* = mol/kg of H_2O) at 463−523 K and 27.5 MPa.

Experimental Section

Within 2 h of use, solutions having 1:1 NH_2OH:HNO_3 were prepared from a stock solution of approximately 50 wt % (16.5 M) hydroxylamine (Howard Hall Division of R.W. Greef and Co.), 70 wt % (15.8 M) nitric acid (Fisher Scientific, ACS), and HPLC-grade water and were stored in a glass container. The flow reactor used[7] permits excellent control of the pressure (±0.1 MPa), temperature (±1.5 K), and flow (±0.01 mL/min, pulseless). The data were collected with a PC that was programmed to control the flow reactor automatically. Such automation permitted multiple data sets to be collected which revealed their overall consistency.

The reaction takes place inside the heated spectroscopy cell constructed of 316 stainless steel (SS) and fitted with sapphire windows.[7] The cell was sealed by compression against a set of gold gaskets whose thickness also controlled the path length (0.0030−0.0045 mm). These seals have limited durability primarily due to the stress of temperature cycling and required occasional disassembly and resealing. The reaction zone of the cell had an internal volume of 0.0604 mL as determined by the cylindrical channel machined through the cell body and the flat duct between the sapphire windows. A transport model of the cell indicated laminar flow and that the solution reaches 85% of the cell temperature well within the first 15% of the entrance tube.[9] The cell/reaction temperature was determined by a K-type thermocouple located in the cell body near the flat duct between the windows.

Experiments were conducted on two concentrations of $[NH_3OH]NO_3$ at 27.5 MPa and with flow rates of 1.79−0.03 mL/min, which resulted in residence times of 2−110 s. A 0.20 *m* $[NH_3OH]NO_3$ solution was studied at four temperatures between 463 and 493 K and 0.10 *m* $[NH_3OH]NO_3$ was studied at seven temperatures between 463 and 523 K. IR spectra (32 summed interferograms, 4 cm^{-1} resolution) were collected with a Nicolet 60 SX FTIR spectrometer using 17 different flow rates at each temperature. After each spectral set was collected and the flow rate was adjusted, the system was stabilized and flushed with at least 10 reactor volumes of sample at the new conditions prior to collection of the next spectral set. Collection of data at each set of flow rates was repeated three times before moving to the next temperature. The cell required resealing after the data sets at the lowest four temperatures were collected on 0.10 *m* $[NH_3OH]NO_3$. A replicate data set was collected at 493 K with the refurbished cell for comparison with the data collected earlier.

Results

Reduction of the spectra to kinetic data required several steps. First, each reaction spectrum was ratioed against the spectrum of pure H_2O in the same cell at the same pressure and temperature to remove as much of the absorption by water as possible. Second, the reactant and product bands were resolved, and areas were calculated by using curve-fitting software (Peakfit, Jandel). The absorbances of interest were fitted with a four-parameter Voigt function. This method permitted accurate integration of the weaker absorptions with the rather poor baselines frequently encountered in IR spectra of water solutions. Third, the absorbances were converted into concentrations at each condition so that the reaction rate could be obtained.

Two distinct absorptions of $[NH_3OH]NO_3$ were observed in the 1800−2900 cm^{-1} window available with sapphire and water.

* Corresponding author.

[⊗] Abstract published in *Advance ACS Abstracts,* October 15, 1997.

S1089-5639(97)02387-6 CCC: $14.00

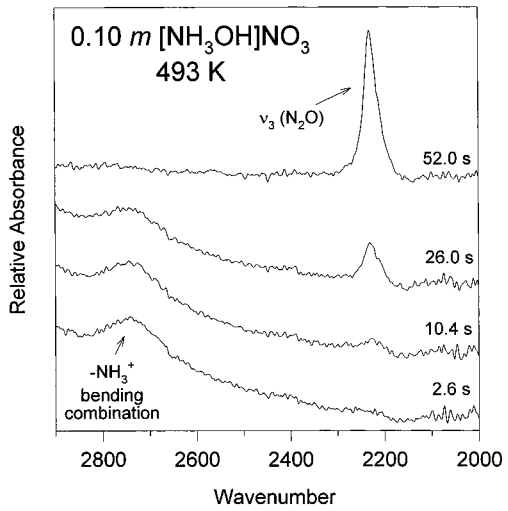

Figure 1. Example infrared spectra of 0.1 *m* $[NH_3OH]NO_3$ at 493 K and 27.5 MPa showing the conversion of the NH_3OH^+ ion ($-NH_3^+$ bending combination) into N_2O(aq) as a function of the residence time.

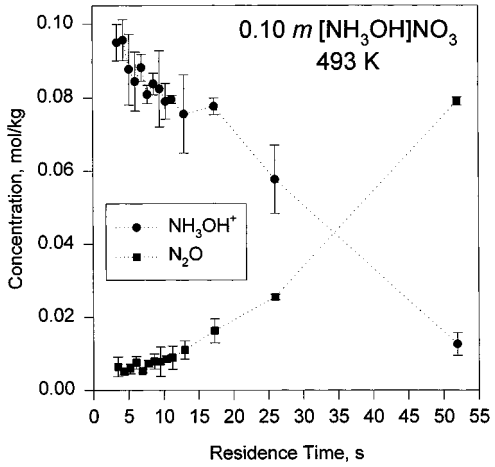

Figure 2. Concentrations of NH_3OH^+ and N_2O as a function of residence time from 0.1 *m* $[NH_3OH]NO_3$ at 493 K under 27.5 MPa. Points represent the average of three data sets, and error bars were determined from the sample standard deviation.

The weak, broad absorption at about 2730 cm^{-1} resulted from the $-NH_3^+$ bending combination mode of the hydroxylammonium ion reactant.[10] A stronger absorption at about 2230 cm^{-1} is the ν_3 stretch of the aqueous N_2O product (Figure 1). The concentrations represented by the integrated band areas were calibrated internally at each temperature.[11] Over most of the temperature range used, the spectra at the shortest residence times indicated no significant reaction and provided an absorbance value for the initial concentration of NH_3OH^+. The absorbance intensity was converted to concentration by assuming Beer's law. In the highest two temperature sets, some decomposition was evident even at the shortest residence times and was taken into account in the analysis. The N_2O concentration was calibrated similarly from the 2230 cm^{-1} band by the fact that complete reaction was achieved at most temperatures in the longest residence time spectra as indicated by the unchanging area of the N_2O band and the absence of the reactant band. Complete reaction was not achieved at the lowest three temperatures, so the area of the N_2O band at completion at a higher temperature was adjusted to account for the density difference of water and then was set equal to the band area at lower temperature. At completion the N_2O concentration is 0.8 of the initial $[NH_3OH]NO_3$ concentration based on the stoichiometry determined by Raman spectroscopy at hydrothermal conditions.[8]

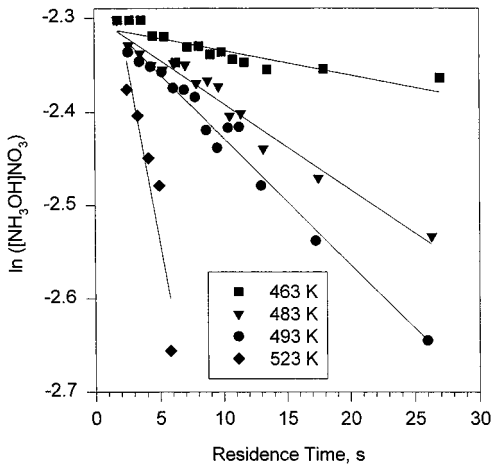

Figure 3. Example of first-order rate plots for the conversion of $[NH_3OH]NO_3$ under 27.5 MPa from the N_2O data at the temperatures shown (see text). Error bars have been omitted for clarity.

TABLE 1: First-Order Rate Constants for NH_3OH^+ Decomposition and N_2O Formation from Aqueous $[NH_3OH]NO_3$

		k, s^{-1} ($\times 10^3$)	
expt[a]	T, K	NH_3^+ bend combination	$\nu_3(N_2O)$
1	463	2.5 ± 0.2	1.6 ± 0.4
2		3.6 ± 0.5	1.7 ± 0.2
1	473	4.3 ± 0.3	3.1 ± 0.1
2		4.0 ± 0.5	4.4 ± 0.3
1	483	11.2 ± 0.5	6.1 ± 0.4
2		13.3 ± 1.6	5.8 ± 1.1
1	493	11.2 ± 1.3	7.7 ± 0.3
2		18.5 ± 1.5	13.7 ± 0.6
3		13.3 ± 2.7	15.5 ± 0.8
3	503	24.6 ± 2.3	17.4 ± 3.5
3	513	26.5 ± 3.3	32.0 ± 5.1
3	523	58 ± 43	43.5 ± 4.5

[a] 1: $[[NH_3OH]NO_3]_0 = 0.20$ *m*; initial seal of cell. 2: $[[NH_3OH]NO_3]_0 = 0.10$ *m*; initial seal of cell. 3: $[[NH_3OH]NO_3]_0 = 0.10$ *m*; second seal of cell.

The collection of multiple data sets permitted determination of the uncertainties in the concentration−time data. Attention was given to the propagation of these uncertainties throughout the kinetic analysis. Each group of three flow rate sets at a particular temperature essentially represented a separate kinetic experiment. Thus, the average concentration ($\bar{x}$) at each flow rate was determined from the three individual measurements, and the uncertainty was determined by the sample standard deviation (s). The averaged concentration data and resulting uncertainties were then plotted against the residence time which was calculated by dividing the reactor volume given above by the flow rate. The reaction profiles result, such as are shown in Figure 2. The flow rate was corrected for the difference in the density of water at each temperature.

The N_2O concentration was converted to conversion of $[NH_3OH]NO_3$ by $[[NH_3OH]NO_3]_0 - ([N_2O]_t/0.8)$, and the kinetic analysis was performed separately on the reactant and the product data using both zeroth- and first-order rate equations. Zeroth-order plots of concentration vs time and first-order plots of ln(concentration) vs time were constructed up to approximately 60% conversion. The first-order plots are shown in Figure 3. The rate parameters were determined from the slope of weighted-least-squares regression (WLSQR) of the averaged concentration data weighted by their uncertainties. In the first-order kinetic analysis, uncertainties were translated into log space as $s/\bar{x}$.[12] The values of k and the resulting uncertainties are listed in Table 1.

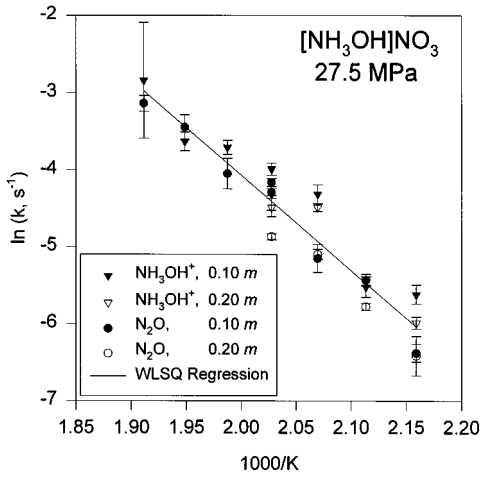

Figure 4. An Arrhenius plot of all of the rate constants in Table 1.

The Arrhenius plot of the first-order rate parameters is shown in Figure 4. The WLSQR of the rates of disappearance of NH_3OH^+ and the appearance of N_2O were both calculated at the 95% confidence interval. The error bars assigned to each rate constant on the Arrhenius plot represent the precision of the individual rate measurements and do not represent the uncertainty in their accuracy. The uncertainty of the rate at each temperature is better represented by the uncertainties of the slope and intercept of the WLSQR of all the data shown in the Arrhenius plot.

Reaction Pathway. Extensive work has been devoted to learning about the mechanism of the reactions of $[NH_3OH]NO_3$ in aqueous solution.[3,8,10,13−26]

$$4[NH_3OH]NO_3 \rightarrow 3N_2O + 7H_2O + 2HNO_3 \qquad (1)$$

The limiting stoichiometry of (1)generally describes a 1:1 ratio of NH_2OH and HNO_3.[13−15] At 420−470 K under 27.5 MPa pressure, the Raman scattering intensities of N_2O and NO_3^- in 0.87−1.74 *m* $[NH_3OH]NO_3$ are consistent with the slightly different stoichiometry of (2).[8] It is known, however, that both the limiting stoichiometry and the reaction details depend on the conditions of the experiment.[14]

$$4[NH_3OH]NO_3 \rightarrow 3.2N_2O + 7.2H_2O + 1.6HNO_3 + 0.4O_2 \qquad (2)$$

The details of the $NH_2OH-HNO_3$ reaction have mainly been probed with a low concentration of NH_2OH in the presence of a large excess of HNO_3.[14,16−21] This condition enables the reaction to be investigated at 273−308 K and minimizes the amount of heat released. It is generally agreed that both HNO_3 and HNO_2 competitively oxidize NH_2OH by reactions 3 and 4.

$$NH_2OH + 2HNO_3 \rightarrow 3HNO_2 + H_2O \qquad (3)$$

$$NH_2OH + HNO_2 \rightarrow N_2O + 2H_2O \qquad (4)$$

Reaction 3 is most important at small NH_2OH:HNO_3 ratios, whereas (4) is increasingly prevalent as this ratio increases.[17,19] The decomposition of $[NH_3OH]NO_3$ is accelerated by the formation of HNO_2.[14,17,18,23] Nonlinear behavior in the form of two stationary reaction states also occurs at small NH_2OH:HNO_3 ratios.[20] Additional mechanism details have been provided by ^{15}N and ^{18}O isotopic labeling studies.[23−26]

As a result of maintaining the NH_2OH:HNO_3 ratio at one in the current work, a mechanism analysis in the sense of most previous work was not conducted. Also, the behavior of only two variables, the reactant NH_3OH^+ and product N_2O, are observable in the 1800−2900 cm^{-1} spectral window available (Figure 1). On the other hand, a 1:1 ratio of NH_2OH:HNO_3 has the widest practical application.[1−3]

A pathway of the decomposition of $[NH_3OH]NO_3$ in water leading to (1) is given by reactions 5−8.[17]

$$NH_3OH^+ + NO_3^- \underset{k_{-1}}{\overset{k_1}{\rightleftharpoons}} NH_2OH + HNO_3 \qquad (5)$$

$$NH_2OH + HNO_3 \xrightarrow{k_2} HNO_2 + H_2O + HNO \qquad (6)$$

$$2HNO \xrightarrow{k_3} N_2O + H_2O \qquad (7)$$

$$2(NH_2OH + HNO_2 \xrightarrow{k_4} N_2O + 2H_2O) \qquad (8)$$

Steady-state treatment of HNO, HNO_2, and NH_2OH yields the rate equation (9).

$$-\frac{d[NH_3OH]}{dt} = \frac{2k_1k_2}{k_{-1} + 2k_2}[NH_3OH][NO_3] \qquad (9)$$

The decreasing bulk dielectric constant of H_2O with increasing temperature[27] favors the right side of eq 5, i.e., k_1 increases relative to k_{-1} as the temperature increases. If $k_{-1} \ll k_2$,then eq 9 reduces to $k_1[NH_3OH][NO_3]$. For the special case of $[NH_2OH] = [HNO_3]$, the rate is expected to have apparent first-order behavior in $[NH_3OH]NO_3$. The same expression applies to $d[N_2O]/dt$. In Figure 2 the profiles for depletion of NH_3OH^+ and formation of N_2O derived from the IR absorbances closely track one another. The incompleteness of the mechanism (5)−(8) at other conditions is evident, however, when excess NH_2OH or HNO_3 is added. For NH_2OH:HNO_3 of 1.0:0.5, the rate indeed decreased by about 0.5, as expected. A 1:2 ratio, however, increased the rate by much more than 2 (i.e., about 10 ± 3). These results are qualitatively consistent with the role of a catalytic species, such as HNO_2, whose concentration increases as the HNO_3 concentration increases.[19]

Arrhenius Kinetics. The activation energy, E_a, for reaction 3 was reported to be 107 kJ/mol from the temperature rise during reaction in the 289−308 K range.[14] E_a for (4) was estimated[14] to be 65 kJ/mol at 273−298 K from the rate of change of the UV absorbance of NO_2^-. More recently, the time-to-reaction method based on thermal explosion theory was applied to aqueous solutions of $[NH_3OH]NO_3$ at 420−470 K under 27.5 MPa.[8] The results indicated $E_a = 129 \pm 29$ kJ/mol for 0.76−1.52 *m* solutions and $E_a = 66 \pm 8$ kJ/mol for 1.58−1.74 *m* solutions. The initial stage of gas evolution from solid $[NH_3OH]NO_3$ is described by eq 10,[28] where E_a is in kJ/mol.

$$k\,(s^{-1}) = 10^{4.6}e^{-69/RT} \qquad (10)$$

Isothermal measurements of species concentrations are difficult to conduct with $[NH_3OH]NO_3$ because of the rapid formation of heat during the reaction. To succeed in the current work, it was necessary to use ⩽0.2 *m* solutions because the heat generated was sufficiently small so as to be controlled by the cell. The concentration−time profiles for which Figure 2 is representative provide rates of conversion in the 463−523 K range. These data fit the first-order rate expression of eq 9 as is shown in Figure 3. It was found, however, that a zeroth-order rate plot gave a statistically equivalent fit. Zeroth-order behavior could be rationalized by assuming that the decomposition of $[NH_3OH]NO_3$ is mainly wall-catalyzed. However, a previous decomposition study of $[NH_3OH]NO_3$ in the hydro-

thermal regime revealed only a small difference in the rate in a 316 SS cell compared to a Ti cell.[8] This result suggests that wall catalysis is not a major factor, which makes zeroth-order kinetics a less appropriate description for the hydrothermal regime. Alternatively, the complexity of the rate constant in eq 9 may be responsible for the absence of a simple order behavior. We have no method to probe the individual steps of (5)−(8) in the hydrothermal regime.

Table 1 lists the first-order rate constants treated statistically as discussed above. The precision in the rate constants is generally satisfactory, but it is apparent that an uncertainty of a factor of 2 or less exists in the accuracy on the basis of the differences incurred when the cell was dismantled and reassembled. This degree of uncertainty in the accuracy of rate constants is in line with our past experience in reaction rate measurements at hydrothermal conditions.[7,8,29] A possible explanation is that flow-rate changes occur from an occasional phase separation (bubble) somewhere in the flow path. A phase separation did not take place in the observation region because no gaseous N_2O was detected.

Figure 4 shows the Arrhenius plot for NH_3OH^+ destruction and N_2O formation. The rates of these processes were statistically indistinguishable and are, therefore, included together on the same plot. The resulting values of $E_a = 103 \pm 21$ kJ/mol and $\ln(A/s) = 21 \pm 5$ are obtained. This value of E_a lies close to that previous estimated for reaction 3 at 292−308 K,[14] but no preexponential factor was previously available. It is also in the range of 129 ± 29 kJ/mol given previously based on the thermal explosion method for <1.5 *m* solutions of $[NH_3OH]NO_3$.[8] These results suggest that the components of $[NH_3OH]NO_3$ react by (3), itself a complex process, and that (3) controls the overall rate. At higher concentrations of $[NH_3OH]NO_3$, the autocatalysis, possibly by the HNO_2 thus formed, accelerates the rate of reaction and release of heat, giving a lower apparent activation energy, i.e., 66 ± 8 kJ/mol.[8]

Relation to Combustion. Some of the mechanistic and kinetic details discussed above appear to apply to very concentrated solutions and to solid $[NH_3OH]NO_3$.[10,22,23,28,30] In particular, accelerating rate observed is consistent with autocatalysis. A type of nonlinear behavior is also noted in the formation rate of the decomposition gases from pyrolysis of >12 M solutions of $[NH_3OH]NO_3$ upon flash heating under 3.5 MPa of Ar.[10] At high concentrations, however, the gaseous products frequently include N_2, NO, and NO_2,[10,22,23,30] but the latter two products can form by various secondary reactions in mixtures containing HNO_2 and HNO_3.[31] The activation energy for solid $[NH_3OH]NO_3$ (eq 10)[28] resembles that for eq 4,[14] which is consistent with the catalytic role of a species such as HNO_2. The rate constant of eq 10 and the kinetics determined in this article are the same at 408 K, which is reasonable on the basis of the roughly similar temperature range in which they were measured.

From the practical point of view, however, it is useful to know whether the kinetics of reaction 2 for a dilute solution or eq 10 for solid $[NH_3OH]NO_3$ apply to the combustion of concentrated $[NH_3OH]NO_3$ solutions. With an estimated surface temperature[5] of 600 K for a burning solution of 9.1 M $[NH_3OH]NO_3$, the kinetics of neither eq 10 ($k = 4 \times 10^{-2}$ s^{-1}) nor Figure 4 ($k = 1$ s^{-1}) are fast enough. The model rate constants required to fit the burning rate of 5−9 M $[NH_3OH]NO_3$ solutions[5] are in the range of $k = 2 \times 10^4$−2.2×10^5 s^{-1}. Thus, we concluded that the rate of decomposition of $[NH_3OH]NO_3$ is suppressed either by the large excess of H_2O in 0.1−0.2 *m* $[NH_3OH]NO_3$ or by the virtual absence of H_2O as in the solid $[NH_3OH]NO_3$. When the $[NH_3OH]NO_3$ concentration is low, reaction 4 cannot dominate, and heat will not be generated at a fast enough rate to sustain burning. In the absence of H_2O, it is possible that the transport properties and concentrations of the key catalytic species are too low to accelerate the rate in the stage of the reaction studied. Only when the $[NH_3OH]NO_3$ concentration is 5 M or higher do all of the necessary properties for fast reaction become sufficiently optimized to sustain combustion. As a result, the global Arrhenius parameters yielding the appropriate rates to model the combustion process of concentrated $[NH_3OH]NO_3$ solutions are most likely the result of a different rate-controlling process than exists below 475 K. In any case the Arrhenius parameters for the combustion regime are probably a mixture of transport rates and reaction rates in the heated surface reaction zone.

Acknowledgment. We are grateful for support of this work by the Army Research Office on the URI Project DAAL03-92-G-0174. The sample of hydroxylamine in H_2O was generously supplied by Hugo Galletta of Howard Hall Division, R.W. Greeff & Co.

References and Notes

(1) Klein, N.; Freedman, E. *Proc. JANNAF Propuls. Mtg.* **1984**, *2*, 287.

(2) Klein, N. *Prog. Aeronaut. Astronaut.* **1988**, *109*, Chapter 14.

(3) *Liquid Propellant XM46 Handbook;* Dowler, W. L., Ferraro, N. W., Eds.; ARDEC: Picatinny Arsenal, NJ, July 1994.

(4) Vosen, S. R. *Combust. Sci. Technol.* **1989**, *68*, 85.

(5) Shaw, B. D.; Williams, F. A. *Proceedings of the 24th Symposium (International) on Combustion;* The Combustion Institute: Pittsburgh, PA, 1992; p 1923.

(6) Klein, N.; Freedman, E. *19th JANNAF Combust. Mtg.* **1982**, *1*.

(7) Kieke, M. L.; Schoppelrei, J. W.; Brill, T. B. *J. Phys. Chem.* **1996**, *100*, 7455.

(8) Schoppelrei, J. W.; Kieke, M. L.; Brill, T. B. *J. Phys. Chem.* **1996**, *100*, 7463.

(9) Schoppelrei, J. W.; Kieke, M. L.; Wang, X.; Klein, M. T.; Brill, T. B. *J. Phys. Chem.* **1996**, *100*, 14343.

(10) Cronin, J. T.; Brill, T. B. *J. Phys. Chem.* **1986**, *90*, 178.

(11) Schoppelrei, J. W.; Brill, T. B. Unpublished results.

(12) Cvetanovic, R. J.; Singleton, D. L. *Int. J. Chem. Kinet.* **1977**, *9*, 481.

(13) McKibben, J. M.; Bercaw, J. E. USAEC, DP-1248, 1971.

(14) Pembridge, J. R.; Stedman, G. *J. Chem. Soc., Dalton Trans.* **1979**, 1657.

(15) Klein, N. ARBRL-TR-02471, Ballistic Research Laboratory, Aberdeen Proving Ground, MD, Feb 1983.

(16) Morgan, T. D. B.; Stedman, G.; Hughes, M. N. *J. Chem. Soc. B* **1968**, 344.

(17) Gowland, R. J.; Stedman, G. *J. Inorg. Nucl. Chem.* **1981**, *43*, 2859.

(18) Bennett, M. B.; Brown, G. B.; Maya, L.; Posey, F. A. *Inorg. Chem.* **1982**, *21*, 2461.

(19) Gowland, R. J.; Stedman, G. *J. Chem. Soc., Chem. Commun.* **1983**, 1038.

(20) Horváth, A.; Póta, G.; Stedman, G. *Int. J. Chem. Kinet.* **1994**, *26*, 991.

(21) Bourke, G. C.; Stedman, G. *J. Chem. Soc., Perkin Trans.* **1992**, *2*, 161.

(22) Lee, H. S.; Thynell, S. T. 33rd AIAA/ASME/SAE/ASEE Joint Propulsion Conference, AIAA97-3232, Seattle, WA, July 1997.

(23) Oxley, J. C.; Brower, K. R. *SPIE* **1988**, *872*, 63.

(24) Bothner-By, A. A.; Friedman, L. *J. Chem. Phys.* **1952**, *20*, 459.

(25) Clusius, K.; Effenberger, E. *Helv. Chim. Acta* **1955**, *38*, 1834.

(26) Hussain, M. A.; Stedman, G.; Hughes, M. N. *J. Chem. Soc. B* **1968**, 597.

(27) Uematsu, M.; Franck, E. U. *J. Phys. Chem. Ref. Data* **1980**, *9*, 1291.

(28) Ratveev, V. A.; Rubszov, U. E. *Izv. Akad. Nauk Ser. Khim.* **1993**, *11*, 1897.

(29) Maiella, P. G.; Brill, T. B. *J. Phys. Chem.* **1996**, *100*, 14352.

(30) van Dijk, C. A.; Priest, R. G. *Combust. Flame* **1984**, *57*, 15.

(31) Kaiser, E. W.; Wu, C. H. *J. Phys. Chem.* **1977**, *81*, 187.